Journal of Current Science and Technology, September-December 2024 Vol. 14 No. 3, Article 73
 ISSN 2630-0656 (Online)

Cite this article: Dang, H. A., Nguyen, V. S., Tran, V. D., Dai, X. L. Hoang, T. N., Quach, T. H., Do, P. N., Nguyen, T. P. D. (2024). Optimal design of a bandpass cavity filter with WR229 input/output by integrating the coupling matrix technique with the trust-region framework. *Journal of Current Science and Technology*, *14*(3), Article 73. https://doi.org/10.59796/jcst.V14N3.2024.73

Journal of Current Science and Technology

Journal homepage: https://jcst.rsu.ac.th

Optimal Design of a Bandpass Cavity Filter with WR229 Input/Output by Integrating the Coupling Matrix Technique with the Trust-Region Framework

Hoang Anh Dang[1], Van Son Nguyen[1,*], Van Dung Tran[2], Xuan Loi Dai[3], Trong Nghia Hoang[1], Thi Hanh Quach[1], Phuong Nhung Do[1], and Thi Phi Doan Nguyen[1]

[1]Faculty of Electrical and Electronic Engineering, Hanoi Open University (HOU), Hanoi, Vietnam
[2]Institute for Technology Development Media and Community Assistance (IMC), Hanoi, Vietnam
[3]Military Institute of Science and Technology, Hanoi, Vietnam

*Corresponding author; E-mail: sonnv@hou.edu.vn

Received 15 April 2024; Revised 11 June 2024; Accepted 14 August 2024
Published online 1 September 2024

Abstract

This study introduces a bandpass waveguide cavity filter designed for the C-band, centered at 3925 MHz. The design employs an efficient method that integrates two techniques: coupling matrix synthesis and the Trust-Region Framework algorithm for optimization. This combined approach provides a good balance between model simplicity and efficiency while maintaining the robustness and accuracy of the designed filter. Simulation results indicate that the filter achieves a return loss of $|S11| \leq -20$ dB and an insertion loss of $|S21| \geq -0.05$ dB. Additionally, the filter demonstrates a rejection level of -50.6 dB at 3000 MHz and -21.9 dB at 5000 MHz. The optimized filter's dimensions in the simulation are 140 × 58.17 × 29.21 mm.

Keywords: *bandpass filter; coupling matrix; trust-region framework; optimization; waveguide; cavity resonator*

1. Introduction

In any communication system, the bandpass filter is a crucial passive component. It primarily allows signals to pass within a specific frequency band, functioning as a gatekeeper. These filters are typically integrated into both the transmitter and receiver of system devices, making them essential components. They aim to minimize return loss and insertion loss within the passband while achieving sufficient rejection power at frequencies outside the passband. This dual functionality makes them essential in communication systems. Over time, filter theory, including bandpass filters, has attracted significant attention from global researchers. As various references (Cristal, 1964; Getsinger, 1962; Puglia, 2000; Wyndrum, 1965) suggest, it has become a robust foundation for myriad design techniques.

Several efficient methods exist for designing and tuning bandpass filters in simulation. These include transformation from lowpass prototype elements (Puglia, 2000; Puglia, 2001), extracting coupling matrix errors (He et al., 2016; Hunter, 2001; Levy et al., 2002), space mapping (Brumos et al., 2014; Melgarejo et al., 2022; Wolansky, & Tkadlec, 2011), and port-tuning (DeMartino, 2018; Swanson, 2020; Swanson, & Wenzel, 2001). These methods have been successfully applied to a wide range of filter topologies (AbuHussain, & Hasar, 2020; Basavarajappa, & Mansour, 2018; Yang et al., 2020).

The transformation from lowpass prototype elements (Puglia, 2000; Puglia, 2001) involves designing an initial lowpass filter and converting it into the desired filter type. The filter type transformation might include lowpass to highpass, lowpass to bandpass, and lowpass to bandstop. This method is fundamental in filter design, but the final design is not optimized, making it less suitable for complex filter design.

In extracting coupling matrix errors (He et al., 2016; Hunter, 2001; Levy et al., 2002), the following steps are included: Initial setup (starting with a simulated S-parameter matrix of the filter); Vector fitting (approximating the S-parameters with a rational function to accurately model the filter's frequency response; Coupling matrix extraction (from the fitted S-parameters, extracting the coupling matrix using analytical or numerical method); and Error minimization (adjusting the coupling coefficients iteratively to minimize the error between the measured and desired responses). Designers must tune the filter over numerous iterations and carefully observe the variation of each coupling matrix component, making filter tuning time-consuming. In many cases, the initial simulated parameters of the filter are not optimal, so additional tools are required for further tuning to get the desired parameters. These tools might include machine learning and deep learning algorithms. Design completion time can take from 7 to 25 minutes or longer, depending on the model of the deep learning algorithm used.

The space mapping method (Brumos et al., 2014; Melgarejo et al., 2022; Wolansky, & Tkadlec, 2011) is a powerful and widely used filter design technique. It requires the following steps with the appropriate model in each step: Coarse model (an approximate description of the filter); Fine model (high-fidelity physics model); Linear mapping (establishment of a linear relationship between the two models using a large set of samples); and Optimization process (optimize the coarse model; transfer the results to the fine model for validation; if necessary, update the coarse model iteratively based on the fine model's behavior). The authors applied five different space mapping techniques to four different filter designs. The results showed that the time to complete the design ranges from 17 min 35 s to 6 h 22 min 20 s. This method ensures good accuracy but requires time-consuming effort, complex calculation models, and the knowledge and experience of designers.

The port-tuning method (DeMartino, 2018; Swanson, 2020; Swanson, & Wenzel, 2001) is a good choice for complex filter design. The method typically involves the following steps: Initial setup (insert multiple tuning ports into the filter design); EM analysis (performing a single comprehensive EM analysis on this multi-port layout); Circuit theory tuning (connection of tuning elements to the tuning ports using circuit theory and their adjustment to achieve the desired filter response); and Real-time adjustments (making real-time adjustments to the tuning elements to fine-tune the filter's performance). This method is suitable for designing microstrip miniature filters and other highly complex designs. However, it requires adding various tuning elements such as capacitors and inductors at each resonator and the space between them before tuning, making the modeling and adjustment of each element's values time-consuming. The time required for a filter design can be up to 1 working day.

There is a balanced approach between model simplicity and efficient convergence while maintaining accuracy in filter design, it is the Trust-Region Framework (TRF) optimization algorithm. The trust-region framework algorithm is crucial in cavity filter design, especially for optimizing performance. It identifies the optimal design parameters that meet specific criteria by iteratively adjusting them within a reliable "trust-region". This algorithm enhances the design process by offering a robust, efficient, and precise optimization method (Blanchet et al., 2019; Diouane et al., 2023; Regis, 2016). The TRF algorithm accelerates the optimization process due to searching only in a certain region around some starting points. However, TRF has strong global convergence, ensuring that the optimization process does not get stuck in local minima.

The issue is the trust-region method depends on the quality of the initial filter model. If the model is too simplistic, it may not yield the best final filter design parameters. Therefore, here the matrix coupling synthesis can assist in creating the initial filter model.

Another potential technique used in microwave filter design is the coupling matrix. In filter design, coupled resonators are interconnected elements (such as resonators, cavities, and waveguides) that influence each other's behavior. The coupling matrix characterizes how energy is transferred between resonators.

The coupling matrix plays a critical role in the design and analysis of filter networks, especially in microwave filter applications. This method allows consideration of the electrical characteristics of each element, including the Q values for each resonator cavity and the different dispersion characteristics for various types of mainline and cross-coupling within the filter (Levy et al., 2002; Puglia, 2001). This technique is not new, but it remains a fundamental starting point for our design.

In this paper, a combination of the coupling matrix and TRF algorithm is used to design a C-band cavity filter.

2. Objectives

The main objective of this work is to introduce a robust and efficient method that combines trust-region framework optimization and coupling matrix synthesis for a bandpass cavity filter design in simulation. The filter has typical characteristics for the 5G communication system and C-band applications. It includes WR229 input/output ports and operates within the range of 3650-4200 MHz.

The first strategy involves using the coupling matrix synthesis, which enables precise modeling and prediction of the filter's behavior. The second strategy involves applying effective optimization techniques, which allow automatic and rapid adjustment of the filter's performance. This two-pronged approach not only simplifies the design process but also significantly improves the overall performance of the filter, and it proves particularly efficient for filters with unique structures. The final design parameters can be achieved while minimizing the time and effort required for the tuning and optimization process.

3. Materials and methods

The proposed method is applied to the design of a C-band cavity filter. The cavity filter is designed based on the WR229 waveguide, using copper and aluminum materials. These materials are suitable for C band frequency, with the cut-off frequency of the lowest order mode being 2.577 GHz and the cutoff frequency of the upper mode at 5.154 GHz.

Our design method is optimized using a two-pronged approach. Initially, the coupling matrix synthesis is used to precisely model and predict the filter's behavior. Following this, an advanced optimization technique is applied, allowing us to fine-tune the filter's performance with a good balance between accuracy and speed. The proposed methods are discussed in the following subsections.

3.1 Coupling Matrix Synthesis

The first step of the filter's design is to determine the initial specifications such as center frequency, bandwidth, and insertion loss. The initial specifications for the target filter are provided in Table 1 below. Next, the coupling matrix is synthesized. The coupling matrix enables the creation of compact and efficient filters with specific frequency responses.

Table 1 Initial specifications for the target filter

Resonator type	Cavity
Frequency	3650 - 4200 MHz
Insertion loss ($\|S_{21}\|$)	≤ –1 dB
Return loss ($\|S_{11}\|$)	≤ –20 dB
Rejection ($\|S_{21}\|$)	≤ –45 dB @3000 MHz ≤ –20 dB @5000 MHz
Input/Output	WR229
Total dimensions	≤ 150 × 105 × 80 [mm]

These specifications anticipate that the filter will incorporate cavity resonators and can be used in 5G communication systems and C-band applications operating within the range of 3650-4200 MHz. Although the requirements for insertion loss, return loss, and rejection are not strict, two major challenges arise. The first challenge involves connecting the cavity resonators to the input/output terminals of the standard WR229 waveguide, which measures 58.17 × 29.26 mm. The second challenge pertains to the physical dimensions of the filter. Specifically, the filter must not exceed 150 × 105 × 80 mm, which corresponds to $1.96\lambda_0 \times 1.37\lambda_0 \times 1.05\lambda_0$, where λ_0 represents the wavelength at the center frequency, f_0 = 3925 MHz.

Given the specifications outlined above, it is evident that a 4th-order filter is required. The coupling matrix has the following form (Hong, 2011):

$$M = \begin{bmatrix} 0 & m_{S1} & m_{S2} & m_{S3} & m_{S4} & m_{SL} \\ m_{1S} & m_{11} & m_{12} & m_{13} & m_{14} & m_{1L} \\ m_{2S} & m_{21} & m_{22} & m_{23} & m_{24} & m_{2L} \\ m_{3S} & m_{31} & m_{32} & m_{33} & m_{34} & m_{3L} \\ m_{4S} & m_{41} & m_{42} & m_{43} & m_{44} & m_{4L} \\ m_{LS} & m_{L1} & m_{L2} & m_{L3} & m_{L4} & 0 \end{bmatrix} \quad (1)$$

where m_{ij} is the coupling between two resonators in the M matrix. The "S" denotes the source, and the "L" denotes the load.

Assuming a symmetric filter structure, the coupling matrix can be synthesized accordingly, as (Levy et al., 2002; Puglia, 2001):

$$M = \begin{bmatrix} 0 & 1.0587 & 0 & 0 & 0 & 0 \\ 1.0587 & 0 & 0.9348 & 0 & 0 & 0 \\ 0 & 0.9348 & 0 & 0.7131 & 0 & 0 \\ 0 & 0 & 0.7131 & 0 & 0.9348 & 0 \\ 0 & 0 & 0 & 0.9348 & 0 & 1.0587 \\ 0 & 0 & 0 & 0 & 1.0587 & 0 \end{bmatrix}$$

Note that the matrix M will be in 6th order due to the inclusion of source and load (input and output ports), and $CBW_{12} = CBW_{34}$ and $Q_{eS} = Q_{eL}$ due to the symmetry of the filter. The resonant frequencies f_i (f_1, f_2, f_3, f_4), internal coupling bandwidths (CBW_{12}, CBW_{23}, CBW_{34}), and external quality factors (Q_{eS}, Q_{eL}) can be derived from the coupling matrix M. These parameters are calculated as follows (Hong, 2011):

$$f_i = \sqrt{f_{start} f_{stop}} \tag{2}$$

$$Q_e = \frac{\sqrt{f_{start} f_{stop}}}{(f_{stop} - f_{start}) m_{S/L,i}^2} \tag{3}$$

$$CBW = m_{ij}\left(f_{stop} - f_{start}\right) \tag{4}$$

where f_{start} and f_{stop} are the start and stop frequencies of the bandpass filter given in Table 1, and $m_{S/L,i}$ is the element 1.0587 in the matrix M. Based on Eq. (2)-(4) and the theory of the matrix M, the reference parameters of the ideal filter are calculated: $f_1 = f_2 = f_3 = f_4$ = 3915 MHz, Q_e = 6.2373, $CBW_{12} = CBW_{34}$ = 523.51 MHz, and CBW_{23} = 399.31 MHz. Then, these parameters will be used for the optimization process.

For clarity, the definitions of filter parameters used in the tuning and optimization process are provided in Table 2.

Based on the initial specifications of the filter in Table 1, the structure of an individual resonator within the filter must be selected first. As depicted in Figure 1, each resonator consists of a conductive rod, with a height of h_0, positioned at the center of a hexagonal air cavity. This arrangement establishes the standard resonant mode. A tuning screw, with a length of l, is situated above the rod to adjust the resonant frequency. It is worth noting that the cross-section of the air cavity can take various shapes, such as a circle, triangle, or rectangle. However, a hexagonal shape is beneficial when arranging the resonators into a triangular lattice. This arrangement optimizes the use of design space during the construction of the entire filter.

Table 2 The filter parameters for the tuning and optimization process

Parameters	Roles
h_0	The height of a conductive rod of each resonator
l	The length of the tuning screw situated above the rod to adjust the resonant frequency
a_0, b_0, c_0, d_0	The dimensions of an air block located between the resonator and the WR229 port
g_0	The distance of the tuning screw at the center
w	The width of the tuning screw at the center
p	The length of the tuning screw at the center

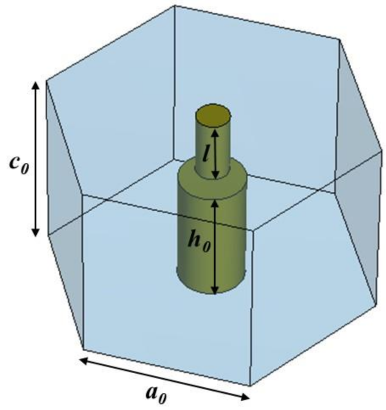

Figure 1 Single resonator with its design parameter

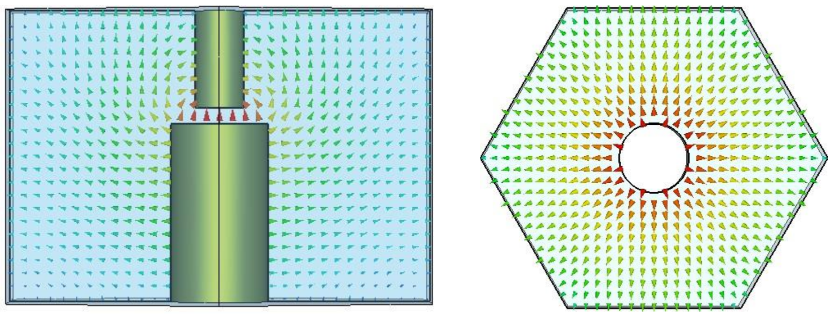

(a)

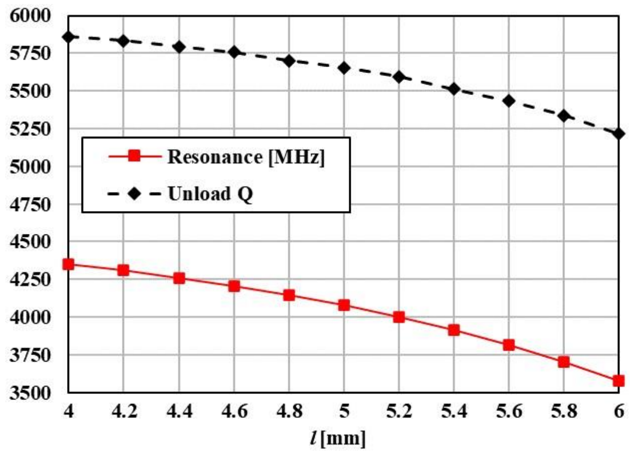

(b)

Figure 2 Property of single resonator: (a) electric field distribution and (b) unload quality factor and resonant frequency

The operation principle of the single resonator is revealed by the electric field distribution, as shown in Figure 2a. It is evident that the electric field is strongly induced in the space between the tops of the rod and the screw, resulting in the standard resonant mode of the resonator. By adjusting the length l of the tuning screw, the frequency of this standard resonant mode can be easily controlled.

Figure 2b illustrates the variation in both the resonant frequency and the unloaded quality factor Q_u based on the length l of the tuning screw, given that a_0 = 15 mm, c_0 = 18 mm, and h_0 = 11 mm. It's clear that as l increases, both the unloaded quality factor and the resonant frequency shift to lower values, with their variations appearing nearly linear. To achieve a resonant frequency of f_0 = 3915 MHz, the length of the tuning screw should be approximately l = 5.37 mm. In this case, the unloaded quality factor is Q_u = 5525, which is sufficiently large to achieve a desirable range of insertion loss for the entire filter, as will be discussed later.

Next, our attention turns to the couplings between the resonators themselves and the input/output ports. The internal coupling between the resonators is examined in Figure 3. As depicted in Figure 3a, the coupling bandwidth (CBW) generated by two adjacent resonators is primarily controlled by three factors: the distance g_0, the width w, and the length p of the tuning screw at the center. Figure 3b provides an example of this investigation, demonstrating the dependence of the CBW on the width w. It shows that larger values of w correspond to larger values of CBW. This filter design case necessitates a relatively large CBW. Consequently, w also needs to be relatively large. This requirement results in the width of the space between the resonators exceeding twice the value of a_0. To obtain the CBWs of 523.51 MHz and 399.31 MHz, the width w should be set at about 36.53 mm and 30.41 mm, respectively.

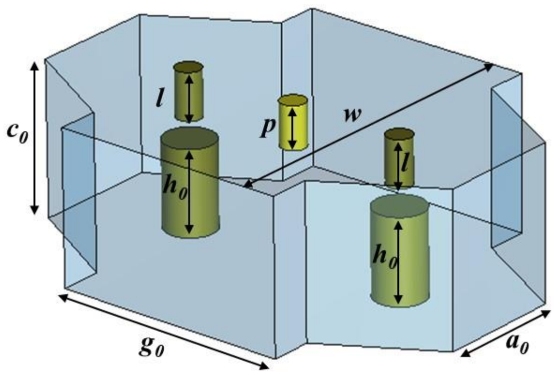

(a)

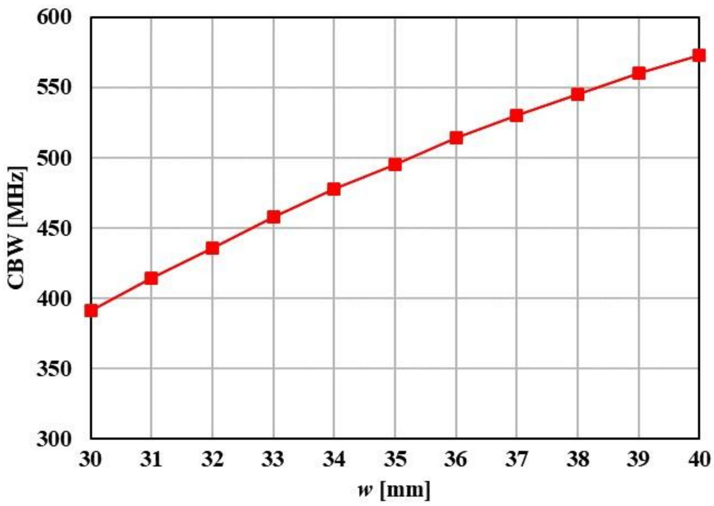

(b)

Figure 3 Internal coupling between two adjacent resonators: (a) simulation model and (b) simulation result

The external coupling between a resonator at the filter's end and the external transmission line (in this case, the WR229 with dimensions of 58.17 × 29.21 mm) is represented by the external quality factor Q_e, as illustrated in Figure 4a. Achieving a low Q_e poses a significant challenge. To address this, we propose the insertion of an air block, with dimensions $b_0 \times c_0 \times d_0$, between the resonator and the WR229 port. A coupling screw, with length p, is positioned within this additional air block to facilitate minor adjustments to Q_e. The effectiveness of this tuning is demonstrated in Figure 4b, where Q_e varies from 5.96 to 6.83 as p is reduced from 7 to 0 mm. To achieve an external quality factor of $Q_e = 6.2373$, the value of p should be approximately $p = 4.5$ mm.

The results of the investigation will serve as the foundation for constructing the complete filter structure. All the dimensional parameters of the filter will be set to the corresponding values of l, w, and p as previously explained.

However, it is important to recognize that the filter's response to this initial approach might not meet the required specifications outlined later. The coupling matrix technique alone is not sufficient to meet the expected specifications and save time and effort. Therefore, further tuning is necessary, leading us to the next optimization strategy, which enables quick and automatic filter tuning.

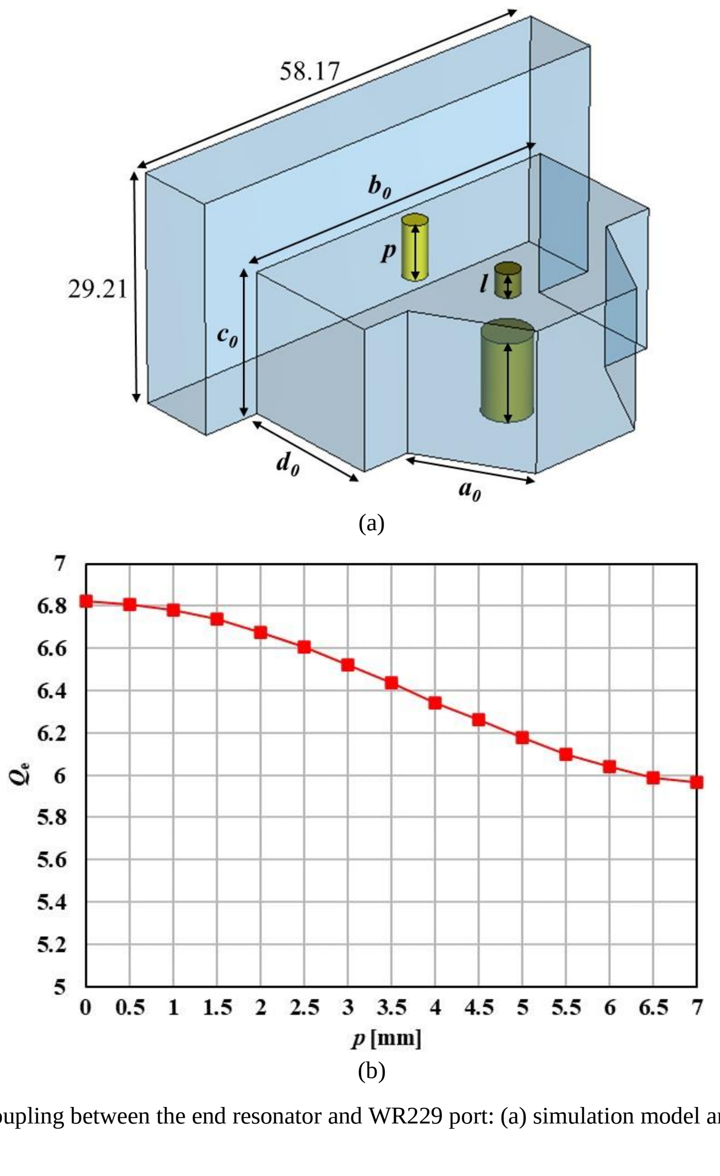

Figure 4 External coupling between the end resonator and WR229 port: (a) simulation model and (b) simulation result

3.2 Trust-region framework optimization

It is important to note that if we rely solely on the coupling matrix technique, the filter response at this stage is not optimal. The return loss is still detuned, and the filter performance is significantly different from the ideal response of the synthesized reference filter.

To achieve the ideal filter response, it is essential to find a simple method that can adjust all design parameters to their optimal values. In this stage, the TRF algorithm is used to find the optimal filter design parameters.

Figure 5 illustrates the complete configuration of the target filter. Some key design parameters are also indicated. In this instance, we maintain fixed distances between the rods while considering the resonator widths (w_{S1}, w_{12}, w_{23}, w_{34}, w_{4L}), the main screw lengths (l_1, l_2, l_3, l_4), and the coupling screw lengths (p_{S1}, p_{12}, p_{23}, p_{34}, p_{4L}) as the design parameters. The distances between the rods are chosen such that the total length of the filter does not exceed 150 mm. In this case, we set this total length to 140 mm, including the two WR229 ports.

The initial values for the design parameters are carefully chosen based on the findings in subsection 3.1.

To begin, the design variables of the optimization process are defined as $X = (x_1, x_2, x_3, x_4, x_5)$, where $x_1 = l_1 = l_4$; $x_2 = l_2 = l_3$; $x_3 = p_{S1} = p_{4L}$; $x_4 = p_{12} = p_{34}$; $x_5 = p_{23}$. Several parameters are chosen to have equal values due to the symmetry in the filter's structure. The widths $w_{S1} = w_{4L}$; $w_{12} = w_{34}$; w_{23} are preset because the tunings of these widths and the coupling screws are identical.

The S_{11} parameter can be defined as (Hong, 2011):

$$S_{11} = \frac{2}{q_{e1}}[\overline{Y}]_{11}^{-1} - 1, \tag{5}$$

where q_{e1} is the scaled external quality factor, $[\overline{Y}]$ is the normalized admittance matrix, which depends on the above design variables. Additionally, we select the maximum value of the return loss S_{11} [dB] within the operation band and denote it as G. Given that the design's target goal is to achieve $|S_{11}| \leq -20$ dB across the entire band, we define the objective function as follows:

$$F(X) = G - G_0, \tag{6}$$

where X is the design variable, and $G_0 = -20$ dB. By minimizing the objective function $F(X)$ to 0 during the automatic optimization process, we can ensure that the return loss across the entire operation frequency band is suppressed to below -20 dB. This ensures that the design goal will be successfully achieved. Our proposed method is demonstrated in the flowchart in Figure 6.

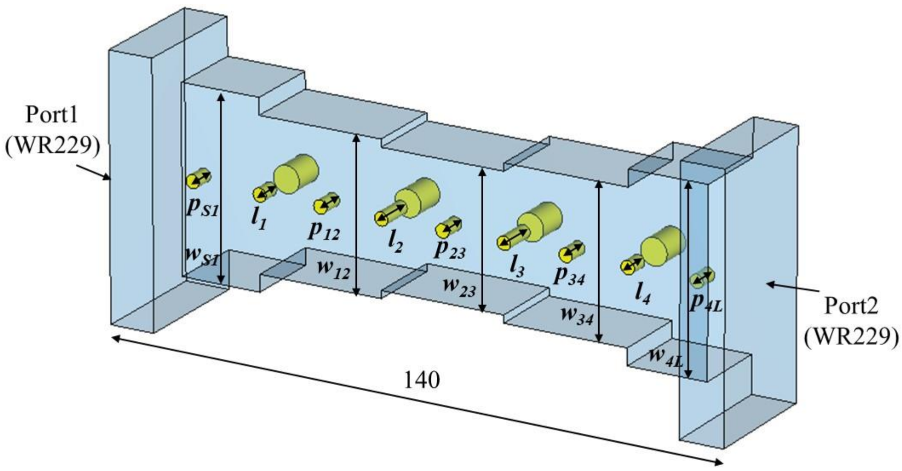

Figure 5 Simulation model of the target filter

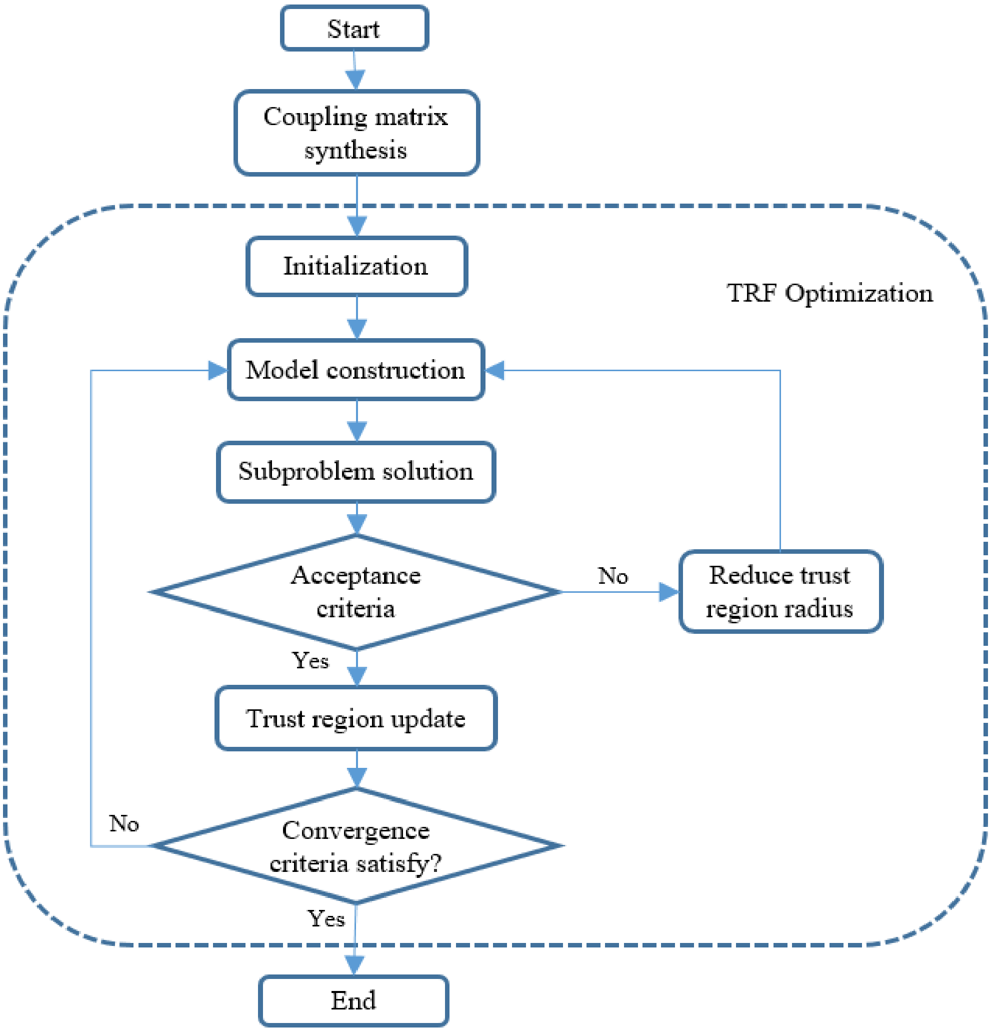

Figure 6 Flowchart of the proposed method

As shown in Figure 6, the flowchart of the proposed method includes two stages. The first stage is the coupling matrix synthesis that was described in the previous subsection. The TRF optimization block in the flowchart involves iteratively solving simpler subproblems within a trust-region around the current solution estimate. It includes the following steps:

- Initialization: start with an initial guess for the solution and set the initial trust-region radius.

- Model construction: Construct a model (quadratic) to approximate the objective function within the trust-region.

- Subproblem solution: Solve the trust-region subproblem to find a step that minimizes the model within the trust-region.

- Acceptance criteria: Evaluate the actual reduction in the objective function and compare it to the predicted reduction. If the reduction is satisfactory, accept the step and move to the next step (update the solution). If not, reject the step and reduce the trust-region radius.

- Trust-regions update: Adjust the trust-region radius based on the performance of the model.

- Termination: Check for convergence criteria. If criteria are met, terminate the algorithm.

- End: Stop and return the current iterate as the final solution.

The TRF is renowned for its rapid convergence and is used here to minimize the objective function $F(X)$ as defined in Eq. (6). The effectiveness of TRF in minimizing $F(X)$ is illustrated in Figure 7. Here,

$F(X)$ started with an initial value of 18.68 at step 1, then quickly decreased and reached 0 at step 29. This indicates that TRF required only 29 optimization steps to successfully achieve the design goal in this case. Additionally, since the optimization process is fully automated, designers can avoid manual tuning steps.

4. Results and discussion

To observe and analyze the variation of return loss during the optimization process, three states of the filter in step 1, step 13, and step 29 are selected for comparison. As shown in Figure 7, the objective function changes significantly at these steps. The dimensions of the filter, specifically the value of the design variable X at these steps, are presented in Table 3, and their S_{11} responses are depicted in Figure 8. The data in Table 3 showed minor variations in X between the three steps, but the plotted lines in Figure 8 revealed clear differences in their responses, indicating that the filter performance was highly sensitive to tuning. While the response at step 1 deviated significantly from the Reference filter, the response at step 13 moved closer to the target frequency band, and the response at step 29 was almost identical to the Reference, satisfying the condition of $S_{11} \leq$ -20 dB across the entire band.

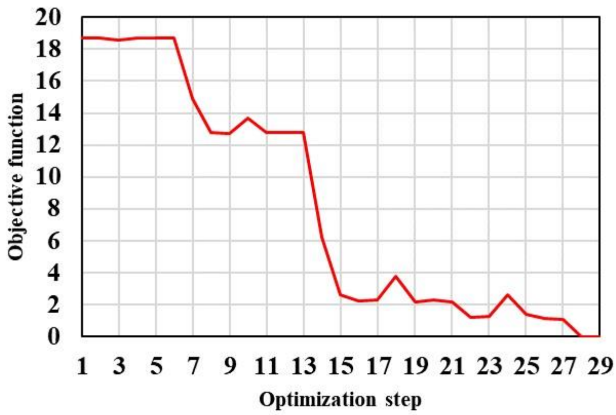

Figure 7 Variation of the objective function

Table 3 Variation of design variable X

Step	x_1 **[mm]**	x_2 **[mm]**	x_3 **[mm]**	x_4 **[mm]**	x_5 **[mm]**
Step 1	4.59	7.25	5.00	4.50	5.50
Step 13	4.73	8.02	4.49	4.37	5.35
Step 29	4.28	7.81	4.86	5.06	4.81

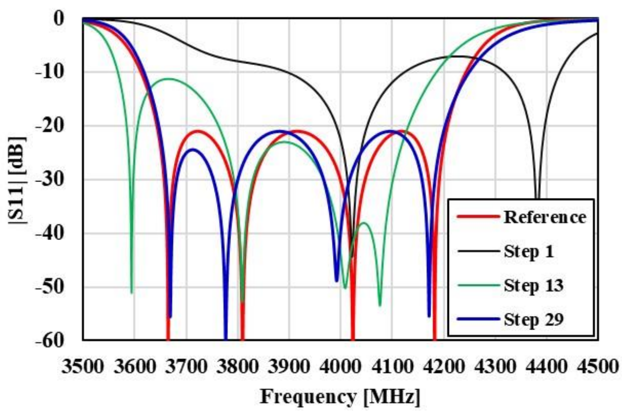

Figure 8 Return loss of the filter design for different tuning steps

As shown in Figure 8, the return loss at step 29 is very close to the reference, but there are some minor differences. Any other termination condition than $S_{11} \leq -20$ dB can be set if necessary. As shown in Table 3, the final filter parameters after TRF optimization are $l_1 = l_4 = x_1 = 4.28$ mm; $l_2 = l_3 = x_2 = 7.81$ mm; $p_{S1} = p_{4L} = x_3 = 4.86$ mm; $p_{12} = p_{34} = x_4 = 5.06$ mm; $p_{23} = x_5 = 4.81$ mm. These parameters allow us to simulate the final filter design in both frequency response and the electric field distribution inside the filter. The TRF optimization process is complete in less than a minute. It is noted that the more parameters the filter has, the more time the optimization process requires. In this design, 29 steps were required to achieve the initial goals. The coupling matrix stage may require additional time to be completed depending on the knowledge and skills of the designers. There are available tools for accelerating this stage, such as Mutual coupling in Matlab.

The final frequency responses of both return loss S_{11} and insertion loss S_{21} are plotted in Figure 9. Figure 9a shows both types of loss on a broad scale, while Figure 9b zooms in on the passband to highlight the ripples in S21. Within the passband, the filter not only achieved a satisfactory return loss of $|S_{11}| \leq -20$ dB but also a commendable insertion loss of $|S_{21}| \geq -0.05$ dB. Outside the passband, the filter exhibited a rejection level of -50.6 dB at 3000 MHz and -21.9 dB at 5000 MHz. While adding more resonators could enhance the rejection zone, our design prioritizes emphasizing the integration of two techniques: coupling matrix synthesis and the trust-region framework algorithm to achieve model simplicity and efficiency.

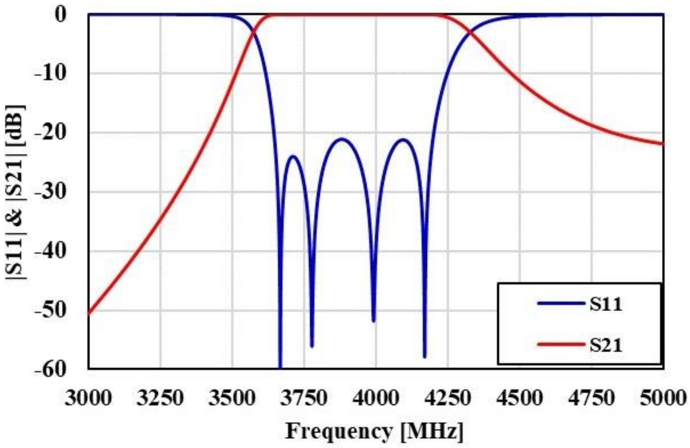

(a)

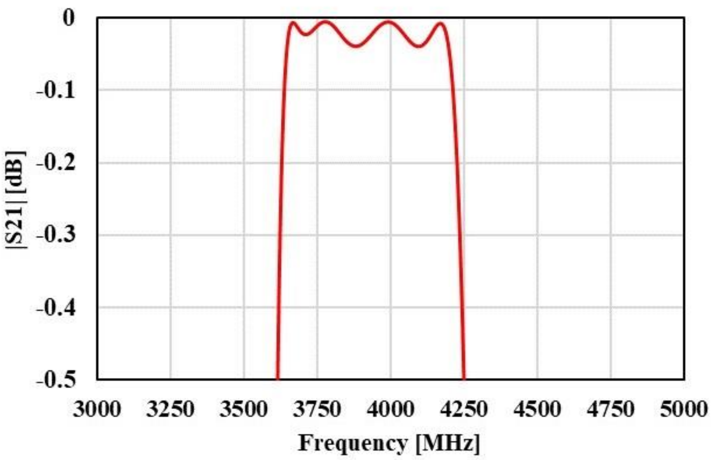

(b)

Figure 9 Final response of the optimized filter: (a) $|S_{11}|$, $|S_{21}|$, and (b) zoomed $|S_{21}|$

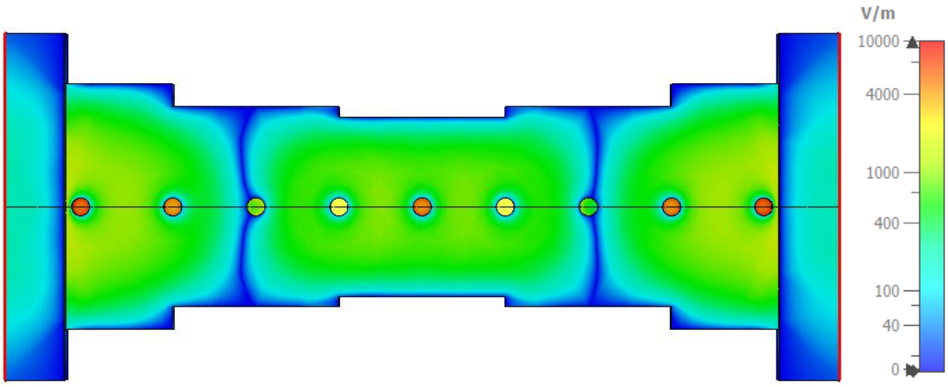

Figure 10 Distribution of electric field inside the optimized filter at center frequency

Figure 10 displays the distribution of the electric field inside the optimized filter at the center frequency of f_0 = 3925 MHz. It can be observed that, due to the filter's symmetric structure, the electric field inside it is also symmetrically distributed. With the input/output terminals of WR229 and the cavity structure, the maximum endurable power of the filter is sufficiently high. Additionally, the total size of the optimized filter in the simulation was 140 × 58.17 × 29.21 mm, meaning that it fully meets the initial design target in Table 1. Although a practical prototype and measured results are not yet available in this paper, these simulation results provide a strong basis for future experimental verification of the filter response, facilitating its application in a practical communication system.

The filter described in this paper stands out due to its distinctive external coupling to waveguide ends, offering low loss and high power endurance. Most importantly, the combination of coupling matrix synthesis and optimization significantly streamlines the simulation-based filter design process, making it quick and user-friendly, even for less experienced designers.

Comparison between methods is relatively difficult because it depends on the complexity of the filter design and the tools used in each method, including software and hardware capabilities. In general, the proposed method can help design a sufficiently effective passband cavity filter with a simple structure (4^{th}-order symmetrical filter), which would require a more complex structure and more time and experience using other methods. For example, the widely used space mapping method (Brumos et al., 2014; Melgarejo et al., 2022; Wolansky, & Tkadlec, 2011) would require additional steps, such as fine model and linear mapping steps for designing the same filter.

This approach is versatile, applicable to any filter type, and particularly effective for designs with numerous tuning variables. More complex filter design scenarios, such as 6^{th}-order filters and nonsymmetric structures, will introduce a larger number of variables to the optimization algorithm which requires more time for the optimization process. In this case, the proposed method serves as an additional option for designers.

5. Conclusion

This paper presented a combination of coupling matrix synthesis and trust-region framework optimization for designing a bandpass cavity filter operating from 3650 to 4200 MHz. The simulation results show that the filter has a return loss of $|S11| \leq -20$ dB and an insertion loss of $|S21| \geq -0.05$ dB. It also exhibits a rejection level of -50.6 dB at 3000 MHz and -21.9 dB at 5000 MHz. The optimized dimensions of the filter in the simulation are 140 × 58.17 × 29.21 mm.

The design process involved synthesizing the coupling matrix to provide a starting model, predicting the filter's behavior, and using advanced optimization techniques to fine-tune its performance efficiently. This approach streamlines the design and improves the filter's overall performance. The filter is unique due to its external couplings to standard rectangular waveguide ports, offering low loss, high power endurance, and compact size, making it ideal for practical applications.

Our next phase involves transitioning from simulation to practical application by fabricating a prototype of the filter and conducting thorough tests to assess its performance in real-world conditions.

6. Acknowledgements

This study was funded by project code MHN2022-01.24 from the HaNoi Open University.

7. References

AbuHussain, M., & Hasar, U. C. (2020). Design of X-bandpass waveguide Chebyshev filter based on CSRR metamaterial for telecommunication systems. *Electronics*, *9*(1), Article 101. https://doi.org/10.3390/electronics9010101

Basavarajappa, G., & Mansour, R. R. (2018). Design methodology of a tunable waveguide filter with a constant absolute bandwidth using a single tuning element. *IEEE Transactions on Microwave Theory Techniques*, *66*(12), 5632-5639. https://doi.org/10.1109/TMTT.2018.2873383

Blanchet, J., Cartis, C., Menickelly, M., & Scheinberg, K. (2019). Convergence rate analysis of a stochastic trust-region method via supermartingales. *INFORMS Journal on Optimization*, *1*(2), 92-119. https://doi.org/10.1287/ijoo.2019.0016

Brumos, M., Boria, V. E., Guglielmi, M., & Cogollos, S. (2014, October 06–09). *Correction of manufacturing deviations in circular-waveguide dual-mode filters using aggressive space mapping* [Conference presentation]. 2014 44th European Microwave Conference, Rome, Italy. https://doi.org/10.1109/EuMC.2014.6986511

Cristal, E. G. (1964). Coupled circular cylindrical rods between parallel ground planes. *IEEE Transactions on Microwave Theory Techniques*, *12*(4), 428-439. https://doi.org/10.1109/TMTT.1964.1125843

DeMartino, C. (2018). How port tuning makes filter design more efficient. *Microwaves RF*, *57*(4), 81-85.

Diouane, Y., Picheny, V., Riche, R. L., & Perrotolo, A. S. D. (2023). TREGO: a trust-region framework for efficient global optimization. *Journal of Global Optimization*, *86*(1), 1-23. https://doi.org/10.1007/s10898-022-01245-w

Getsinger, W. J. (1962). Coupled rectangular bars between parallel plates. *IRE Transactions on Microwave Theory Techniques*, *10*(1), 65-72. https://doi.org./10.1109/TMTT.1962.1125447

He, Y., Wang, G., Song, X., & Sun, L. (2016). A coupling matrix and admittance function synthesis for mixed topology filters. *IEEE Transactions on Microwave Theory Techniques*, *64*(12), 4444-4454. https://doi.org./10.1109/TMTT.2016.2614666

Hong, J.S. (2011). *Microstrip filters for RF/microwave applications*. New Jersey, U.S.: John Wiley & Sons. https://doi.org/10.1002/0471221619

Hunter, I. C. (2001). *Theory and design of microwave filters (no. 48)*. Stevenage, U.K.: IET Digital Library. https://doi.org/10.1049/PBEW048E

Levy, R., Snyder, R. V., & Matthaei, G. (2002). Design of microwave filters. *IEEE Transactions on Microwave Theory techniques*, *50*(3), 783-793. https://doi.org/10.1109/22.989962

Melgarejo, J. C., Ossorio, J., San-Blas, A. A., Guglielmi, M., & Boria, V. E. (2022). Space mapping filter design and tuning techniques. *International Journal of Microwave Wireless Technologies*, *14*(3), 387-396. https://doi.org/10.1017/S175907872100146X

Puglia, K. V. (2000). A general design procedure for bandpass filters derived from lowpass prototype elements: Part I. *Microwave Journal-Euroglobal Edition*, *43*(12), 22-38.

Puglia, K. V. (2001). A general design procedure for bandpass filters derived from low pass prototype elements: Part II. *Microwave Journal-Euroglobal Edition*, *44*(1), 114-137.

Regis, R. G. (2016). Trust regions in Kriging-based optimization with expected improvement. *Engineering Optimization*, *48*(6), 1037-1059. https://doi.org/10.1080/0305215X.2015.1082350

Swanson, D. (2020). Port tuning a microstrip-folded hairpin filter [application notes]. *IEEE Microwave Magazine*, *21*(4), 18-28. https://doi.org/10.1109/MMM.2019.2963609

Swanson, D. G., & Wenzel, R. J. (2001, May 20–24). *Fast analysis and optimization of combline filters using FEM* [Conference presentation]. IEEE MTT-S International Microwave Symposium Digest (Cat. No. 01CH37157), Phoenix, AZ, USA. https://doi.org/10.1109/MWSYM.2001.967097

Wolansky, D., & Tkadlec, R. (2011). Coaxial filters optimization using tuning space mapping in CST studio. *Radioengineering*, *20*(1), 289-294.

Wyndrum, R. W. (1965). Microwave filters, impedance-matching networks, and coupling structures. *Proceedings of the IEEE*, 53(7), 766-766. https://doi.org/10.1109/PROC.1965.4048

Yang, J., Zhang, Y., Zhang, D., Hong, T., Liu, Q., Sun, D., Dong, A., & Lv, S. (2020, June 15-19). *Highly selective filter for suppressing interference of 5G signals to C-band satellite receiver* [Conference presentation]. International Wireless Communications and Mobile Computing (IWCMC), Limassol, Cyprus. https://doi.org/10.1109/IWCMC48107.2020.9148404